AGU PUBLICATIONS

JGR

Journal of Geophysical Research: Atmospheres

RESEARCH ARTICLE

10.1002/2013JD019850

Key Points:
- Planetary wave zonal structure derived from network of SuperDARN meteor winds
- Robustness of extracting each zonal component compared to current techniques
- Mesospheric planetary waves used as possible precursor of stratospheric warmings

Correspondence to:
N. H. Kleinknecht,
nora.kleinknecht@ntnu.no

Citation:
Kleinknecht, N. H., P. J. Espy, and R. E. Hibbins (2014), The climatology of zonal wave numbers 1 and 2 planetary wave structure in the MLT using a chain of Northern Hemisphere SuperDARN radars, *J. Geophys. Res. Atmos.*, *119*, 1292–1307, doi:10.1002/2013JD019850.

Received 14 MAR 2013
Accepted 14 JAN 2014
Accepted article online 16 JAN 2014
Published online 13 FEB 2014

The climatology of zonal wave numbers 1 and 2 planetary wave structure in the MLT using a chain of Northern Hemisphere SuperDARN radars

Nora H. Kleinknecht[1], Patrick J. Espy[1,2], and Robert E. Hibbins[1,2]

[1]Department of Physics, NTNU, Trondheim, Norway, [2]Birkeland Centre for Space Science, Bergen, Norway

Abstract The zonal wave components 1 and 2 were extracted from the meridional wind along the latitude band of 51–66°N for the years 2000–2008 using eight Super Dual Auroral Radar Network (SuperDARN) radars spanning longitudes from 25°E to 150°W. Each extracted zonal component represents the superposition of all temporal periods with that zonal structure and indicates the total planetary wave energy available with that wave number. The Hovmöller diagrams show stationary as well as eastward and westward traveling planetary waves propagating in the background wind. The method used to detect the zonal planetary wave components in the SuperDARN data are detailed and validated using UK Meteorological Office data, which allows the evolution of S_1 and S_2 planetary wave energy between the stratosphere and mesosphere to be assessed. The climatology of zonal wave number 1 and 2 planetary wave activity in the mesosphere-lower thermosphere (MLT) is presented and compared to the activity in the stratosphere. The MLT climatology of the mean wind anomalies shows stronger planetary wave activity during winter and weaker activity during summer with enhancement around midsummer and autumn equinox. The climatology of the mean wind displays similar amplitudes apart from very strong S_1 planetary wave amplitudes during summer. In addition planetary wave activity during winters with major and minor stratospheric warming events are examined and contrasted.

1. Introduction

The interaction of radiation, dynamics, and chemistry, coupled with the curvature and rotation of the Earth, creates a complex structure in the atmosphere and a wide range of wave phenomena, such as tides, gravity, and planetary waves, with time scales in the range from a few minutes to several weeks. The cause and effect of planetary wave activity in the mesosphere-lower thermosphere (MLT) is still an open question. Some studies [e.g., *Dowdy et al.*, 2004; *Espy et al.*, 2005; *Chshyolkova et al.*, 2006; *McDonald et al.*, 2011] suggest an extension of the stratospheric wave field. Others found evidence for additional planetary wave activity through in situ generation by dissipation or breaking gravity waves and/or propagation of planetary wave activity from the winter hemisphere or equator to the summer MLT [e.g.,*Williams and Avery*, 1992; *Forbes*, 1995; *Espy et al.*, 1997; *Mitchell et al.*, 1999; *Smith*, 2003; *Garcia et al.*, 2005; *Pancheva et al.*, 2008].

In this study the wind field is separated into zonal wave numbers 1 (S_1) and 2 (S_2). The sum or superposition of all planetary wave modes of zonal structure 1 itself has zonal structure 1 with time-dependent amplitude, similarly for wave number 2. Because the atmosphere responds to the total superposition of all wave energy, not to a single period, wave number or propagation direction, the S_1 and S_2 wave energies have been used as a standard technique to assess the total wave forcing and its zonal character in stratospheric analyses [e.g., *Labitzke*, 1977, 1981; *Bancalá et al.*, 2012]. For that reason it has been adopted here. Not only does it give the total planetary wave energy available (and its longitudinal character), but it may easily be compared with stratospheric wave energy to assess the energy deposited in the background flow and its zonal structure. Comparison of the climatology of zonal wave numbers 1 and 2 planetary wave structures in the MLT and the stratosphere can be used to understand how MLT and stratospheric planetary wave activity are related. In addition, it indicates those seasons where mesospheric waves might be an extension of the stratospheric waves and when they are most likely generated locally in the mesosphere.

Planetary wave activity throughout the middle atmosphere has mainly been studied on a global scale by satellites [e.g., *Belova et al.*, 2008; *McDonald et al.*, 2011]. However, some studies have also used multiple ground-based radar stations to trace the propagation of planetary waves [e.g., *Espy et al.*, 2005; *Baumgaertner et al.*, 2008] and to compare that multiple-station data with satellite observations [e.g., *Bristow*

et al., 1999; *Pancheva et al.*, 2008]. Satellites give the opportunity to scan the whole Earth, making observations of the global behavior of planetary waves possible. The disadvantage of satellites is that they alias spatial and temporal information since it may take between 1 day and several weeks before a given geographic location is sampled at the same local time [e.g., *Wu et al.*, 1995]. In addition, if they operate in a Sun synchronous mode, only one phase of the migrating tide is observed.

Here the zonal wave numbers 1 and 2 planetary wave structures in the MLT have been observed using the Super Dual Auroral Radar Network (SuperDARN) [*Greenwald et al.*, 1985, 1995] around the North Pole operating as a so called "ground-based satellite." It has the spatial resolution required to trace longitudinal wave components, but in contrast to satellites, it also has very good temporal resolution (1 h) for a fixed point on Earth. This makes it possible to remove tides from the data accurately and give a global picture of longitudinal wave components at the latitude band between 51–66° N. Since many of the radars in the SuperDARN network have been in operation nearly continuously since the 1990's, it is possible to utilize a long time series of simultaneous data from 6–8 radars in order to determine individual longitudinal planetary wave components and compose climatologies of these components.

2. Data

SuperDARN radars [*Greenwald et al.*, 1985, 1995] were originally built for observation of the *F* region. Later it was shown [*Hall et al.*, 1997; *Jarvis et al.*, 1999; *Hussey et al.*, 2000; *Yukimatu and Tsutsumi*, 2002] that sporadic echoes received in the first few range gates are due to scatter from the ionization trails left by meteors ablating in the lower thermosphere and upper mesosphere. These trails travel with the neutral wind, which makes it possible to deduce the line of sight wind over the meteor ablation altitudes (80–100 km) [*Hocking et al.*, 2001]. Meteors observed in the lowest range gates of the multiple beams of the SuperDARN radars over $\sim$ 1 h are then combined in order to determine the vector neutral wind at the centroid location of the beams. Standard SuperDARN radars have no altitude discrimination within the lowest range gates used for meteor-trail detection, but the mean altitude of the meteor wind has been estimated to be 94 ($\pm$ 3) km by comparing the derived wind with that observed by a colocated MF radar [*Hall et al.*, 1997]. This has been verified by comparing winds from an imaging Doppler interferometer radar at Halley (75°S, 26°W) and a colocated SuperDARN radar [*Hibbins and Jarvis*, 2008]. Recently, *Chisham and Freeman* [2013] have developed a new method for calibrating SuperDARN interferometric data to estimate the meteor altitudes directly, finding a broad distribution between 75 and 125 km with a peak near 102–103 km. Although the peak of this meteor distribution is higher than the average derived through wind comparisons, *Chisham and Freeman* [2013] have suggested that this discrepancy is likely due to the averaging process. The hourly mean meridional winds and uncertainty estimate (number of meteors) are taken from the SuperDARN data base (http://psddb.nerc-bas.ac.uk/data/access/) and are processed as described in *Hibbins and Jarvis* [2008].

A more rigorous approach in determining accurate mean winds from a single SuperDARN radar would employ interferometric height finding [*Hussey et al.*, 2000] coupled with the techniques outlined in *Yukimatu and Tsutsumi* [2002], *Hussey et al.* [2000], and *Tsutsumi et al.* [2009] to eliminate any sidelobe contamination issues. However, not all the radars currently have this option, and those that do have have not been run continuously in this mode. The data need to be consistent, with good data coverage from one radar to the next and from 1 year to the next in order to attempt the planetary wave analysis. Therefore, in order to maximize the data coverage, while preserving the best longitudinal uniformity, the noninterferometric data was used to derive the mean winds from all radars. Previous studies [*Jenkins et al.*, 1998; *Jenkins and Jarvis*, 1999; *Hibbins and Jarvis*, 2008; *Hibbins et al.*, 2011] have taken this approach to meteor wind analysis and produced effective comparisons on short and long time scales with winds derived from other types of MLT radars that incorporated more conventional range determination of altitude.

The beam patterns of SuperDARN radars are known to have back lobes [*Milan et al.*, 1997], and contamination from meteors observed in the back lobes can lead to an underestimation of mean winds and tidal amplitudes from noninterferometric SuperDARN radars [*Yukimatu and Tsutsumi*, 2002; *Arnold et al.*, 2003]. If the horizontal winds observed in all SuperDARN radars are affected similarly, then the planetary wave amplitudes we derive will be similarly reduced. However, if the back lobe effects on the magnitude of the winds differ between the different radars, this could generate spurious stationary waves. Comparative studies of the mean wind have shown that the back lobe correction factors required for the SuperDARN radars are similar for radars at different locations and with different boresight directions [*Hussey et al.*, 2000; *Arnold*

Table 1. SuperDARN Radars Used in the Data Analysis[a]

Radar	Loc.(Geo)	Loc.(Mag)	Data Cov.
Hankasalmi	64.4 N, 25.2 E	61 N, 116 E	1995–2009
Pykkvibaer	65.7 N, −18.0 E	70 N, 77 E	1996–2008
Stokkseyri	64.7 N, −26.9 E	71 N, 62 E	1994–2008
Goose Bay	55.5 N, −60.3 E	65 N, 16 E	1995–2008
Kapuskasing	51.4 N, −83.3 E	61 N, −15 E	1993–2009
Saskatoon	54.2 N, −105.2 E	62 N, −44 E	1993–2008
Prince George	56.1 N, −123.2 E	61 N, −66 E	2000–2009
Kodiak	59.5 N, −150.1 E	60 N, −96 E	2000–2009

[a]Geographic (geo) and magnetic (mag) mean location (loc.) of scatter and data coverage (data cov.) of the SuperDARN radars used in the data analysis. Longitudinal wave components could only be retrieved during 2000–2008 when the longitudinal coverage was sufficient.

et al., 2003; *Hibbins and Jarvis*, 2008]. However, *Tsutsumi et al.* [2009] show that the meteors distributions seen in the back lobes may be different between the Iceland and Finland SuperDARN radars. Although wind differences induced by such site-specific back lobe effects in the SuperDARN radars have yet to be quantified, they could affect the planetary wave amplitudes derived from longitudinal chains of such radars if they prove to be significant.

Differences in the amplitude of the semidiurnal tide derived from noninterferometric SuperDARN radars and other MLT radar systems can largely be explained by the short vertical wavelength of this tide combined with the poor vertical resolution of the SuperDARN radar winds, with back lobe contamination of the SuperDARN radars playing a negligible role [e.g., *Hibbins et al.*, 2011]. Although there is relatively poorer agreement in the amplitude of the smaller diurnal tide between SuperDARN and other radars, these differences have been ascribed to the diurnal variation in meteor count rate, with low meteor counts in the evening creating large uncertainties in the inferred winds [*Hussey et al.*, 2000; *Thayaparan and Hocking*, 2002].

Table 1 shows the SuperDARN radars used in the study including the centroid location of the beam and years of data coverage used in the data analysis. All SuperDARN radars between 51–66°N with sufficient data coverage are used in the study.

3. Data Analysis

To assure data quality, the raw wind data from all SuperDARN radars used were quality checked before processing. Hourly mean winds above 100 m/s, winds with standard deviations of zero or a mean location different from the geometric centroid of the beams are excluded. These values are either unrealistic solutions or indicate a nonstandard operation mode of the radar [*Hibbins and Jarvis*, 2008]. To extract zonal planetary wave modes from the hourly averaged meridional wind of the eight radar stations, the data are processed through several steps as outlined below.

3.1. Daily Mean Wind

To produce daily mean winds that are not influenced by tides and quasi-two-day waves (QTDWs), data are treated in a similar fashion to *Hibbins and Jarvis* [2008]. First, the hourly mean winds are split into 4 day segments. Then a bias (mean wind) and 8 h, 12 h, 24 h, and 48 h sine waves, representing the strongest tidal components [*Hibbins et al.*, 2006] and the QTDW, are fitted to this segment of hourly winds. To ensure sufficient data coverage for the fit, only segments covering at least half of the hourly means and spanning at least 16 different hours are used [*Hibbins and Jarvis*, 2008]. In addition, 4 day segments that have data gaps >3 h occurring at the same hours in each day are excluded. Similarly, 4 day segments with data gaps >12 h that cover the same hours in both halves of the segment, are rejected. The 4 day segments are then stepped by 1 day intervals to build up a time series of 4 day running mean winds. Monthly averages of the mean wind and the QTDW as well as the amplitudes and phases of the tides for all eight radars are in broad agreement with other climatological observations for similar latitudes [e.g., *Manson et al.*, 1985; *Portnyagin et al.*, 2004; *Chshyolkova et al.*, 2005]. As an example, Figure 1 shows the monthly average fitting result for the meridional component of the wind recorded with the Hankasalmi SuperDARN radar (64°N, 25°E).

The mean wind is clearly equatorward during summer and turns more poleward during winter. The amplitude of the QTDW is observed to increase in summer, in agreement with *Salby* [1981]. The amplitude and phase of the 24 h tide is relatively constant, while the amplitude and phase of the 12 h tide are more variable. During equinox the amplitude of the 12 h tide is smallest and the local time of maximum phase occurs earlier. The amplitude of the 8 h tide is generally small with a maximum in October when the amplitude of the 12 h tide reaches a minimum. During summer the 8 h tide is nearly absent as indicated by small or insignificant amplitudes and nearly random phases. The behavior of the observed phases and amplitudes of

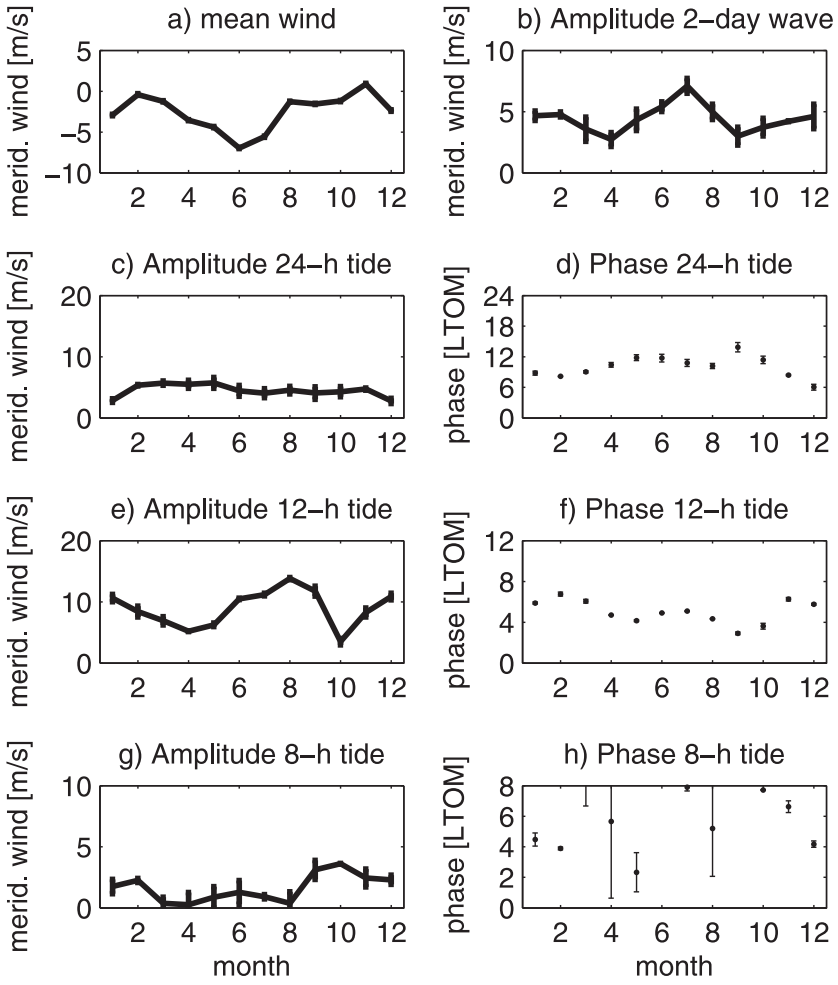

Figure 1. Monthly weighted mean of the mean wind, the 2 day wave and the 24 h, 12 h, and 8 h tides at Hankasalmi. The tidal phase represents the local solar time of the first maximum. The error bars shown are the standard errors of the weighted means.

the tides at Hankasalmi are similar to tides at 95 km altitude observed with an All-Sky Interferometric Meteor Radar at Esrange (68°N, 21°E) [*Mitchell et al.*, 2002]. The smaller tidal amplitude measured by the SuperDARN radars is a common feature that has been attributed to sidelobe effects [*Yukimatu and Tsutsumi*, 2002] or to the combination of the large vertical integration of the SuperDARN radar together with a finite vertical wavelength of the tide [*Hibbins et al.*, 2011].

3.2. Climatology and Daily Mean Wind Anomaly

To eliminate the seasonal variation of the mean wind, a smoothed meridional wind climatology over all years of the daily mean wind was produced for each of the eight radars. To form the climatology for each radar, the individual daily means, $V_{d,y}$, weighted by their individual fitting uncertainties, $\delta V_{d,y}$, were used to calculate the climatology over all years of data available, C_d, as shown in equation (1). Similarly, the corresponding standard error of the mean, δC_d, for each day of the climatology was calculated following equation (2).

$$C_d = \frac{\sum_y \frac{V_{d,y}}{(\delta V_{d,y})^2}}{\sum_y \frac{1}{(\delta V_{d,y})^2}} \quad (d = \text{day}, y = \text{year}) \tag{1}$$

$$\delta C_d = \frac{1}{\left(\sum_y \frac{1}{(\delta V_{d,y})^2}\right)^{1/2}} \tag{2}$$

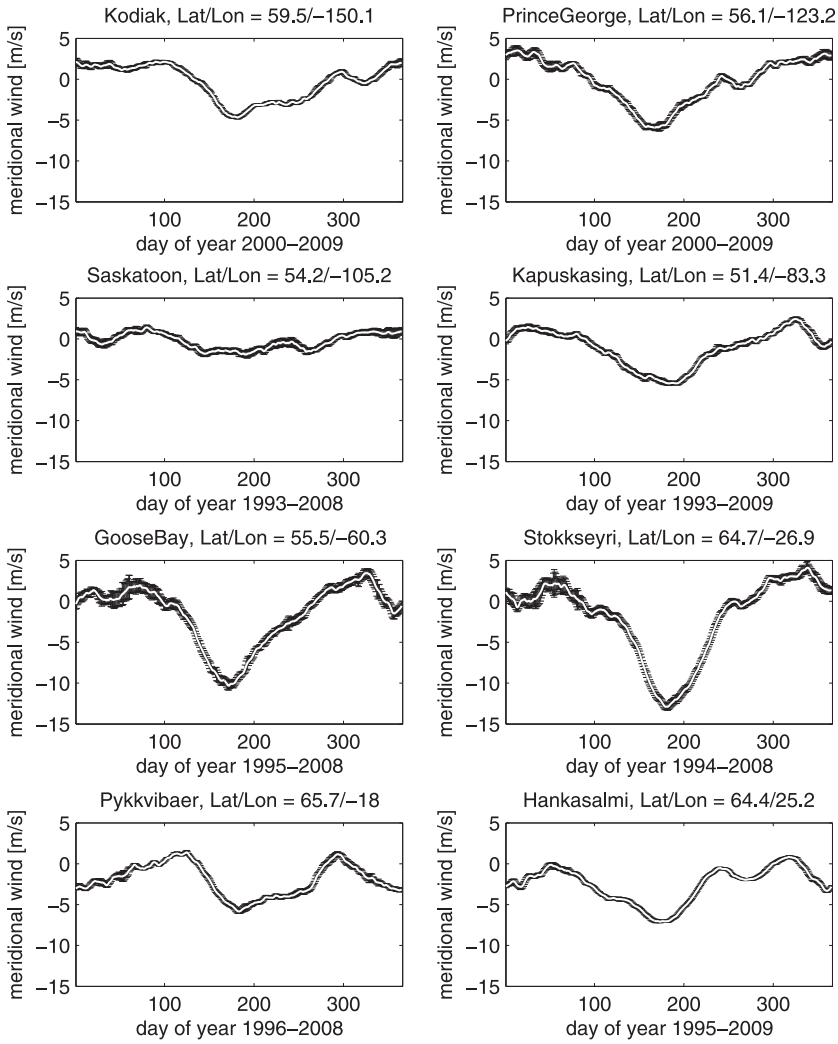

Figure 2. Smoothed (30 day running mean) climatology of all eight radar stations. Weighted mean (white line). Standard error of the weighted mean (black error bars).

A 30 day running mean was used to smooth the resulting climatology in order to remove any vestigial planetary wave effects. Figure 2 shows the smoothed meridional wind climatology for all stations, indicating their locations and the years used for the climatologies. Each day of the climatology includes at least 4 years of data.

Daily mean meridional wind anomalies ($V^{\text{ano}}_{d,y}$) and their estimated uncertainties, $\delta V^{\text{ano}}_{d,y}$, were then created by removing the smoothed climatology (C^{s}_{d}) from the individual daily mean wind data for each radar as shown in equations (3) and (4).

$$V^{\text{ano}}_{d,y} = V_{d,y} - C^{s}_{d} \tag{3}$$

$$\delta V^{\text{ano}}_{d,y} = \sqrt{(\delta V_{d,y})^2 + (\delta C_{d})^2} \tag{4}$$

Both anomaly mean meridional winds and mean meridional winds as a function of longitude are fitted for planetary wave components as described below. A detailed discussion about similarity and difference between the retrieved wave components can be found in section 5.

3.3. Longitudinal Fit

Longitudinal wave components are retrieved by fitting two sinusoids with 360° and 180° spatial periods as a function of longitude to the daily mean wind anomaly at all available radar stations. These fitting components correspond to wave modes with zonal wave number $S = 1$ and 2, respectively. The fit was weighted

with the uncertainty ($\delta V_{d,y}^{\text{ano}}$) of the daily mean wind anomaly given in equation (4). The strongest zonal wave number 3 component (a 120° sinusoid) represents the QTDW [*Salby*, 1981] which has already been removed in the detrending process. Thus, it and higher order waves, are taken to be insignificant and the fitting was stopped at $S = 2$. The zonal wave number $S = 0$ was calculated from the mean of the residual of the fit. Data are only fitted if the westernmost (Kodiak −150.1°) and most easterly (Hankasalmi 25°) stations are present, and at least four additional stations are available with no sequential data gaps (i.e., the missing stations are not located next to each other). The method described above is validated in the next section.

4. Validation

The longitudinal fitting technique used has been validated in three different ways.

4.1. Comparison With the Single Sites

The first validation compares the daily wind anomaly for the time period (1 January 2000 to 31 December 2008) at each station with the sum of the longitudinally fitted zonal wave components (S_1 and S_2) evaluated at the longitude of each station. Only days where both a longitudinal fit and the daily wind anomaly are available at the specific station were compared. The correlation coefficient between the daily wind anomaly and the sum of the fitted zonal components was statistically significant at >99% confidence level and greater than 0.75 at all but one station. The exception was Goose Bay where the correlation coefficient was still 0.61, significant at the 99% level. This high degree of correlation shows that the longitudinally fitted S_1 and S_2 components reproduce the majority of the observed variance in the daily wind at each station.

4.2. Comparison to a Full 360° Longitudinal Fit

A further validation of the technique was done by using meridional wind data from the UK Meteorological Office (UKMO)-Stratospheric Assimilated Data [*Swinbank and O'Neill*, 1994; *Met Office et al.*, 2013] at 6.8 hPa. As with the mesospheric analysis, the stratospheric anomaly meridional wind was calculated by removing a climatology for each longitude (2.5° spacing). A full 360° fit, using 2.5° longitudinal spacing, for the first four zonal wave numbers was done (S_0, S_1, S_2, S_3), at 51°N, 66°N, and for a latitude average between 51 and 66°N. These latitudes correspond to the southernmost, northernmost, and average latitude of the radar stations used in the SuperDARN analysis. Figure 3 (top left, top right, and bottom left) show Hovmöller diagrams for the first three zonal wave numbers during 2002 at 51°N, 66°N, and the average latitude band (51–66°N), respectively. From the similarity between the Hovmöller diagrams of the different latitudes and a correlation coefficient larger than 0.83, it is clear that the 15° latitudinal extent does not have a strong impact on the variability and phase of the S_1 and S_2 components as the phase progression is similar at all latitudes. The resulting amplitude lies between the larger northern and the weaker southern amplitudes. However, one should be aware that such a latitude span will have a larger effect in the midlatitudes and caution should be exercised when applying a similar method to midlatitude radars. Since the Hough functions of the normal modes which make up these wave components are not a function of altitude, the latitudinal extent of the radar chain used in the SuperDARN analysis should not affect the amplitudes and phases retrieved in the MLT. It is also clear from the plot that the S_0 component varies over the latitude band and that it is therefore not possible to retrieve a unique S_0 component.

To verify that the longitudinal extent of the SuperDARN radar network used is adequate to retrieve a zonal wave number $S = 1$ and $S = 2$, the meridional UKMO anomaly wind was sampled at the locations (longitude and latitude) of the radar stations and the wave number components were fit again repeating the aforementioned method. Figure 3 (bottom right) displays the resulting Hovmöller diagram for 2002. The S_3 component was removed from the data before the fit to emulate the removal of the 2 day wave in the SuperDARN winds. To verify this, fits with and without removal of the S_3 component were correlated and show a good agreement (correlation coefficients ≥ 0.83).

The variability, amplitude, and phase progression of the $S = 1$ and $S = 2$ wave number retrieved using only the radar locations compares well with the full, 360° fit. The correlation coefficients between the ideal 360° fits between 51° and 66°N and the fit at the coordinates of the SuperDARN stations for the amplitude and the phase of the zonal wave numbers 1 and 2 components are larger than 0.9 for both wave numbers. This indicates that the fit to the SuperDARN radar winds can accurately capture the temporal changes of the planetary wave components. The amplitude of S_1 retrieved at the stations is approximately 20 ± 20 % higher than the amplitudes retrieved from the ideal fit. The amplitude of the S_2 wave agrees within the 10%

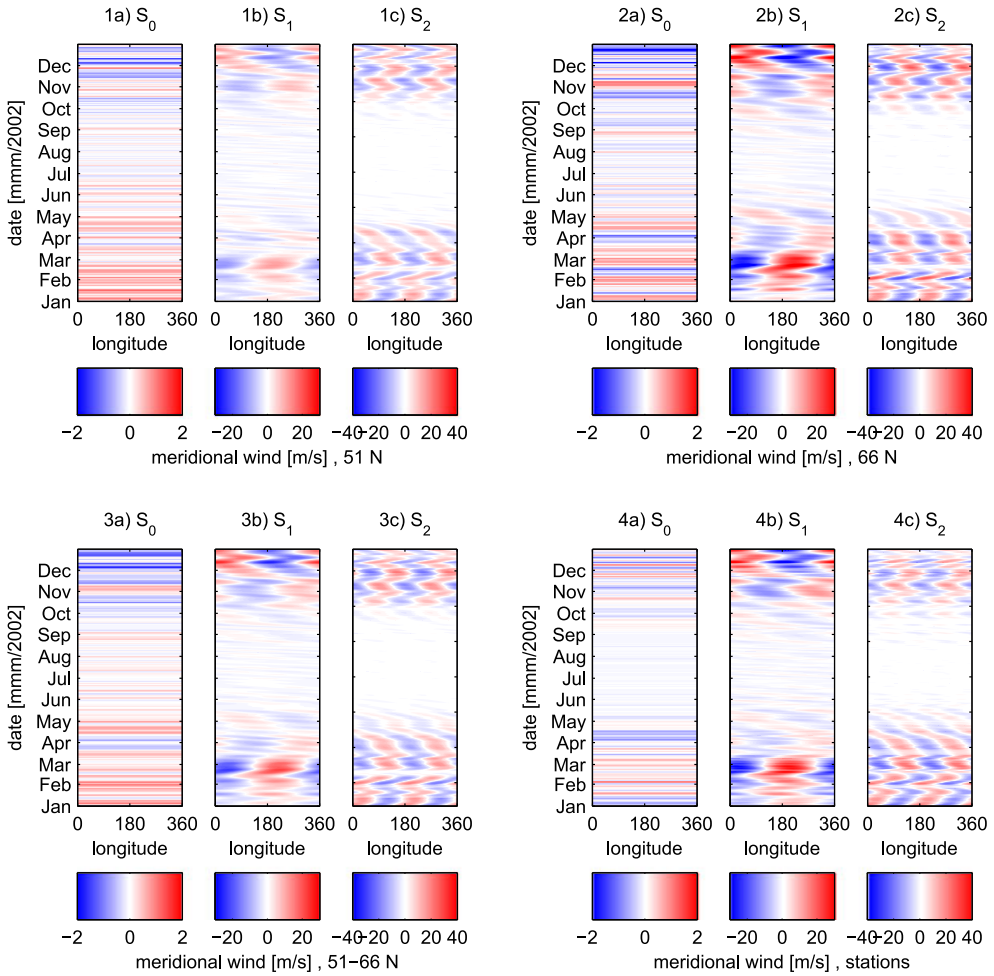

Figure 3. Hovmöller diagram of longitudinal wave components S_0 (a), S_1 (b), S_2 (c)) using the "ideal" longitudinal fit for anomaly meridional UKMO winds (top left) at 51°N, (top right) at 66°N, and for the latitude band (bottom left) 51–66°N for year 2002. (bottom right) Hovmöller diagram of longitudinal wave components using the anomaly meridional UKMO wind only at the coordinates of the SuperDARN chain for year 2002. Red and blue colors signify poleward and equatorward winds, respectively.

uncertainty of the two fits. Thus, the longitudinal extent of the SuperDARN radar stations can accurately reproduce the true amplitude of the S_2 component, but overestimates the S_1 component slightly.

4.3. Comparison to Hydroxyl Rotational Temperatures

For any given longitude, the different temporal components of each zonal wave number can be found by spectral analysis of the time series of the amplitudes and phases of that zonal component using Fourier, Lomb-Scargle, or wavelet techniques followed by band-pass filtering. Similar analysis has been applied to satellite- and ground-based data [e.g., *Grytsai et al.*, 2005; *McDonald et al.*, 2011; *Demissie et al.*, 2013]. While there could be some distortion of the waveform using a band-pass filter, their use to extract planetary waves has been demonstrated [e.g., *Belova*, 2008]. Figure 4 shows the quasi-16-day component of the zonal wave number one (a), two (b), and the sum of both (c) at 18°E for the time period 15 November 2001 to 15 March 2002.

This longitude and time period was chosen because temperatures derived from the hydroxyl (OH) nightglow from Stockholm (59.5°N,18.2°E) are available during that winter [*Espy et al.*, 1997]. To extract the quasi-16-day periodicity from the other wave components, a bidirectional fourth order Butterworth band-pass filter [*Stearns*, 1975] with a band pass between 14 and 18 days was chosen. This filter separates the quasi 16 day periodicity from other strong peaks in the power spectrum. The OH-temperatures at Stockholm can be filtered in the same way, and the extracted quasi-16-day wave can be compared to the sum of the zonal wave components from the longitudinal fit (Figure 4c). It can be seen

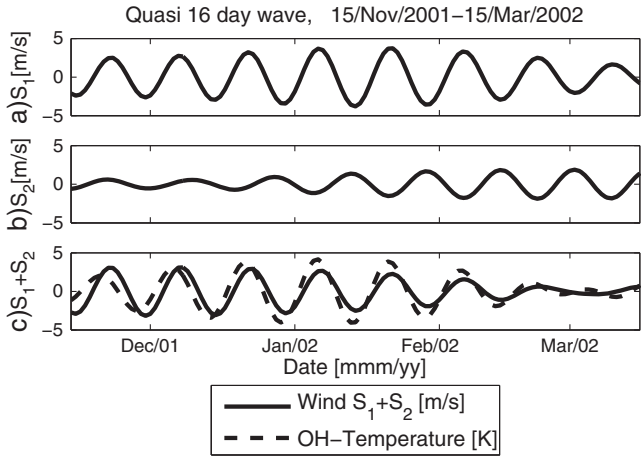

Figure 4. Quasi-16-day wave of the (a) S_1 and (b) S_2 anomaly meridional wind component at 18°E and (c) the sum of both components (solid line) together with the quasi-16-day component of the ground-based OH-temperature observation (dashed line) at Stockholm (59.5°N, 18.2 °E).

that the wave character of the quasi-16-day wave extracted from the wind is dominated by the zonal wave number 1 component and agrees well with the phase and relative amplitude of the wave in the OH rotational temperatures. Observation of the quasi-16-day wave at OH-temperature altitudes (~87 km), at SuperDARN altitudes as well as in the lower stratosphere [e.g., *Alexander and Shepherd*, 2010], and throughout the whole stratosphere and mesosphere during winter [e.g., *McDonald et al.*, 2011] suggest an upward propagation of this wave component from the stratosphere into the MLT region.

5. Results and Discussion

The meridional wind anomalies from eight SuperDARN meteor radars between 51 and 66°N have been used to fit longitudinal planetary wave modes. Each resulting zonally fitted component (here S_1 and S_2) represents the superposition of stationary, as well as propagating and traveling normal mode waves with a variety of temporal periods. Wave components were fitted from January 2000 to December 2008 allowing the seasonal and interannual changes of the total planetary wave activity and its zonal character to be examined. Hovmöller diagrams of the fitted wave components for all years are shown in Figure 5. Red and blue colors signify poleward and equatorward winds, respectively. Throughout the 9 years of data, we typically see larger planetary wave activity during the winter month and weaker, but still significant, planetary wave activity during summer in both zonal wave components (S_1 and S_2). The phase of the zonal components are most stable during the summer months (see Figure 5) suggesting a quasi-stationary wave is the dominant wave component then.

Even though the longitudinal fits to each day's data are independent, Figure 5 shows that the phase of each fitted component is relatively stable from day to day. In addition, the phase can be seen to shift smoothly in time, indicating that the wave component is moving with respect to the ground-based stations. The change in time of the phase and amplitude of each zonal component are the result of both interaction with the background wind and the interaction of the different temporal components. At times the phase of the S_1 and S_2 waves seems to jump 180°, for example, on 3 March 2005. A closer look at these phase changes shows that the 180° phase transition occurs rapidly and systematically over the course of a few days. Similar 180° phase jumps can also be seen in analysis of total ozone from the Total Ozone Mapping Spectrometer [*Grytsai et al.*, 2005] and have been attributed to rapid bursts of the zonal wind speed and interaction of similarly strong eastward and westward wave packets with similar temporal periods.

The meridional wind climatologies at the different stations show large differences, especially in summer as can be seen in Figure 2. To investigate whether this behavior is the result of long-lasting wave features with a phase that is consistent year to year, zonal wave components were also fitted to the daily mean meridional winds, i.e., the winds where the climatologies were not removed. Hovmöller diagrams of the wave components for all 9 years are shown in Figure 6. Red and blue colors signify poleward and equatorward winds, respectively. The wave components are similar in amplitude and phase to the mean meridional wind

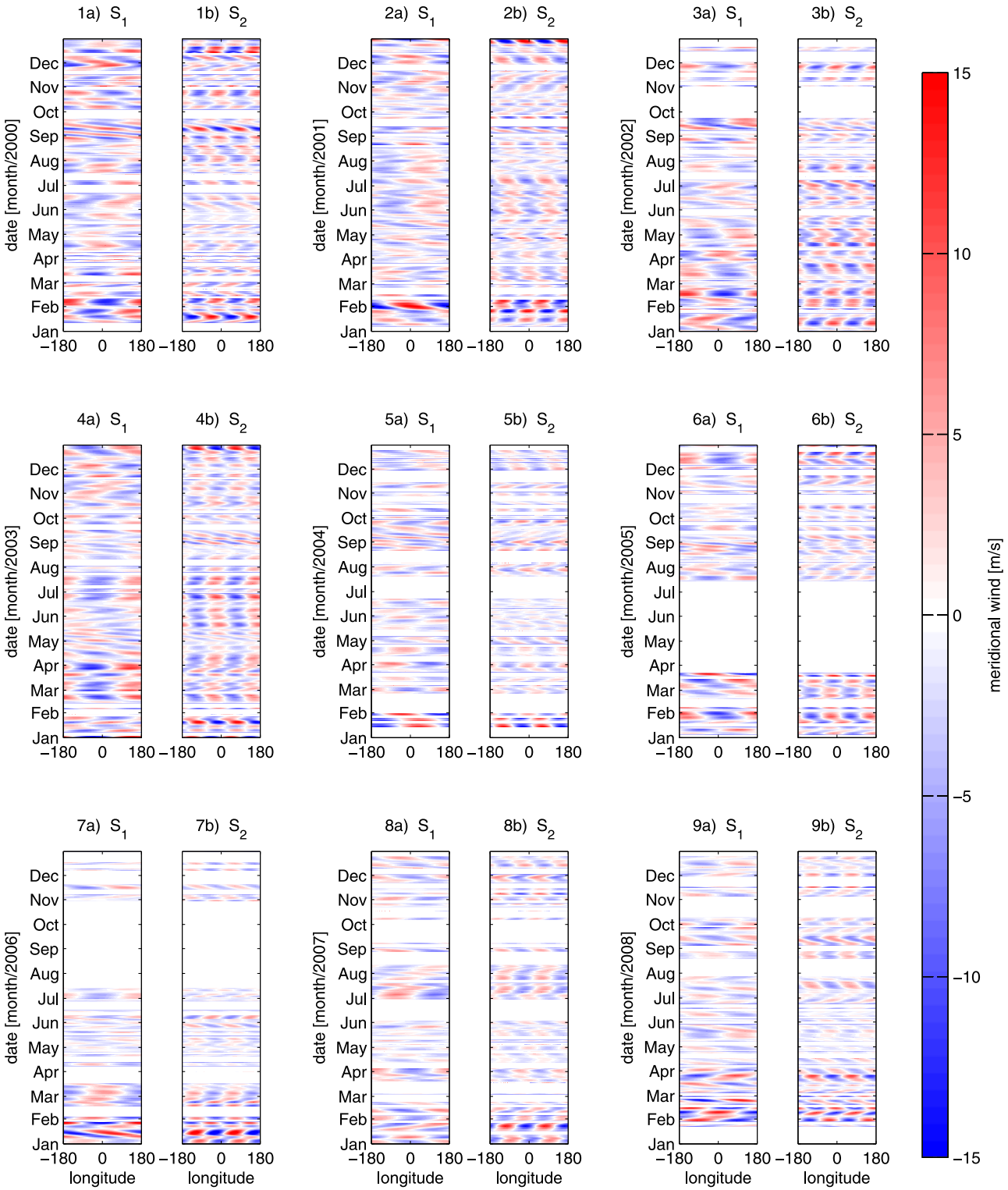

Figure 5. Longitudinal wave components (a) *S*1 and (b) *S*2 of the mean meridional wind anomalies for all years, 2000–2008 (1–9). Red and blue colors signify poleward and equatorward winds, respectively.

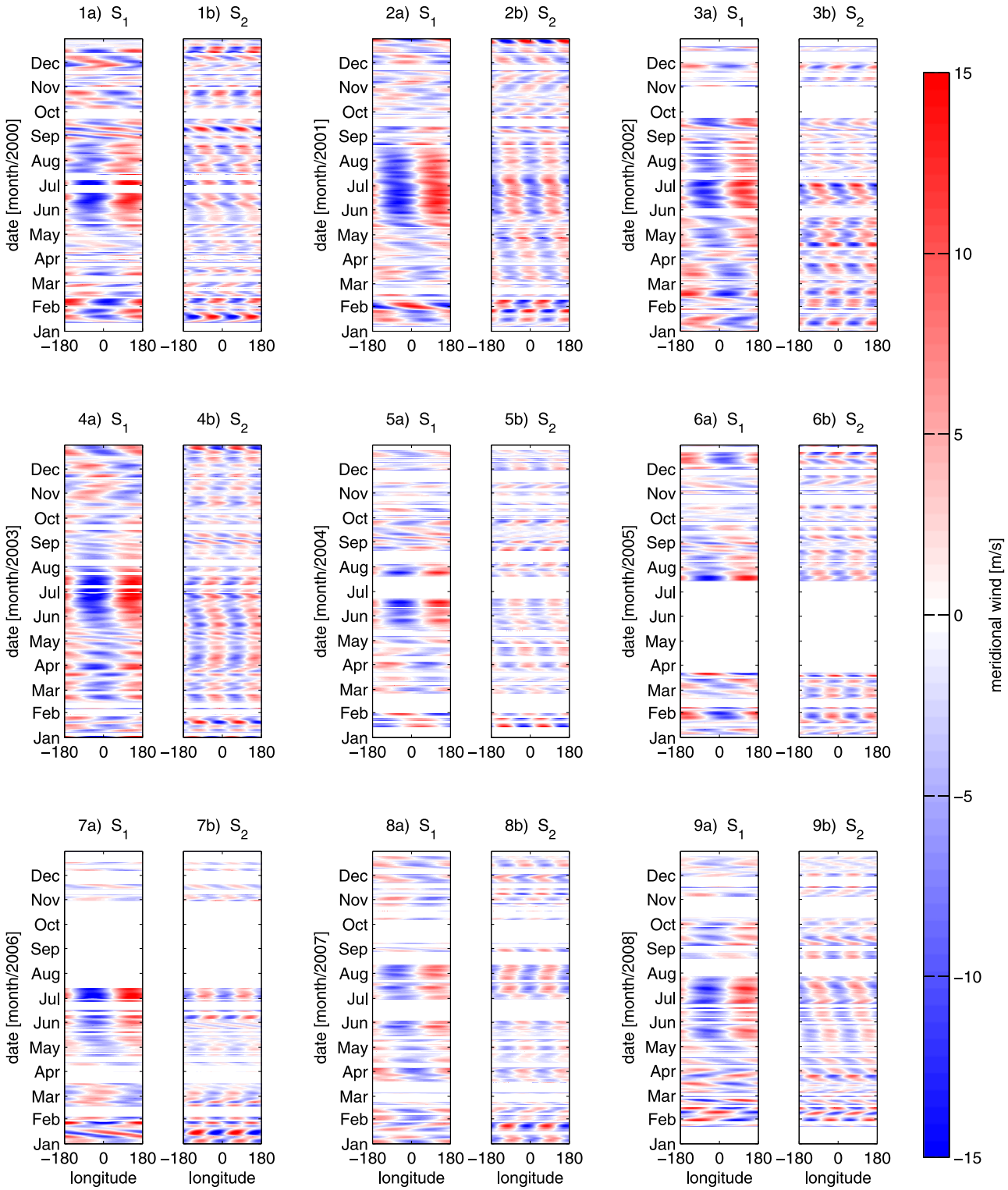

Figure 6. Longitudinal wave components (a) S_1 and (b) S_2 of the meridional wind for all years, 2000–2008 (1–9). Red and blue colors signify poleward and equatorward winds, respectively.

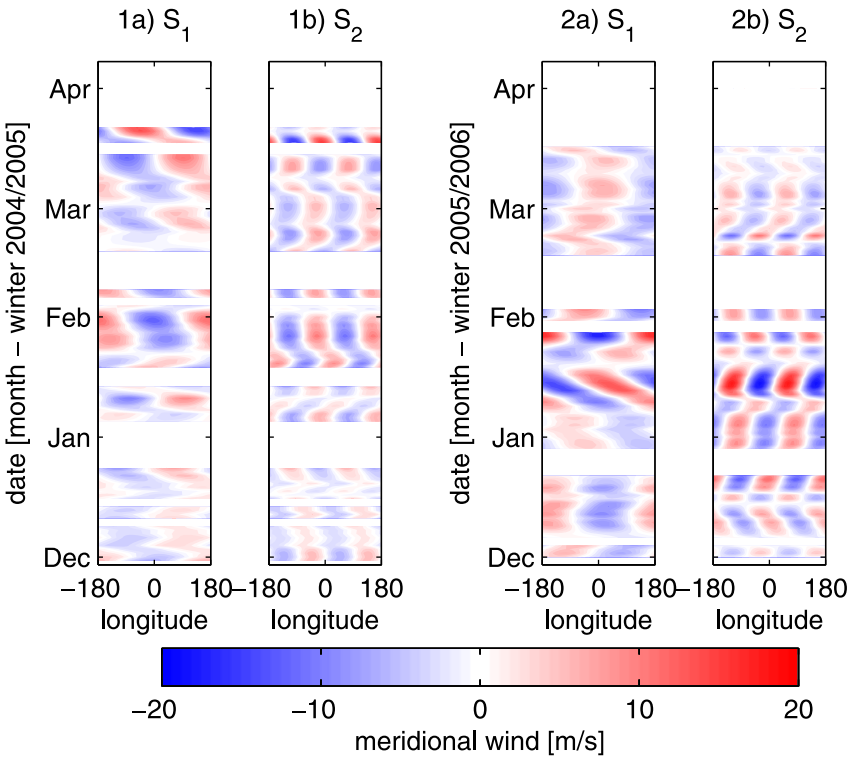

Figure 7. Longitudinal wave components (a) S_1 and (b) S_2 of the mean meridional wind anomalies, for (left) winter 2004–2005 and (right) winter 2005–2006. Red and blue colors signify poleward and equatorward winds, respectively.

anomalies throughout the year apart from the summer season. During all summers a strong stationary wave structure with a phase that is consistent year to year dominates the mean meridional wind wave components. It is unclear if this persistent year-to-year summer time wave structure is a stationary Rossby wave, or if it is produced by longitudinal differences in the gravity wave forcing [*Smith*, 2003]. It may even be the result of the underestimation of the S_0 component resulting from the limited longitudinal range of the radar chain, a limitation that will be relaxed as more SuperDARN radars are added to the chain in the future. The existence of a stationary Rossby wave in the polar summer MLT is puzzling since propagation from below is very unlikely due to the summertime westward stratospheric jet [*Charney and Drazin*, 1961]. However, longitudinally varying gravity wave forcing has been shown to produce planetary wave-like features in the MLT [*Smith*, 2003]. The appearance of a strong stationary S_1 wave only during the summer could be due to the stronger gravity forcing in the summer MLT resulting from the seasonal difference in wave breaking altitudes, i.e., approximately 80 km in summer and 50 km in winter [*Lindzen*, 1981]. Evidence for seasonally persistent S_1-like structures have also been found in other studies of the meridional wind in the MLT region. For example *Dowdy et al.* [2007] observed evidence for similar structures in the climatology of the meridional wind measured using two MF radars in the northern polar region which are approximately 180° apart (Poker Flat and Andenes). The effect maximized at approximately 90 km around summer solstices and approximately 70 km around winter solstices (see Figure 4) [*Dowdy et al.*, 2007]. This seasonal variation with altitude is consistent with gravity wave breaking as the cause of this phase-stable S_1 structure.

5.1. Interannual Planetary Wave Variability

Applying this longitudinal fitting technique to several years of data shows both eastward and westward traveling waves as well as stationary waves. Shown in Figure 7 are examples for the winters (left) 2004/2005 and (right) 2005/2006. Evident in these data is a strong interannual variability of the mesospheric planetary waves that may be associated with stratospheric warming events. For example, the wave activity during the winter of 2005/2006, where a major stratospheric warming was observed [*Manney et al.*, 2009a; *Lima et al.*, 2012], is stronger and more stationary than during the winter of 2004/2005 when only a minor warming occurred. This strong stationary wave activity during 2005/2006 is consistent with the generally weak polar vortex, higher stratospheric temperatures, and high ozone concentrations that occurred in the stratosphere

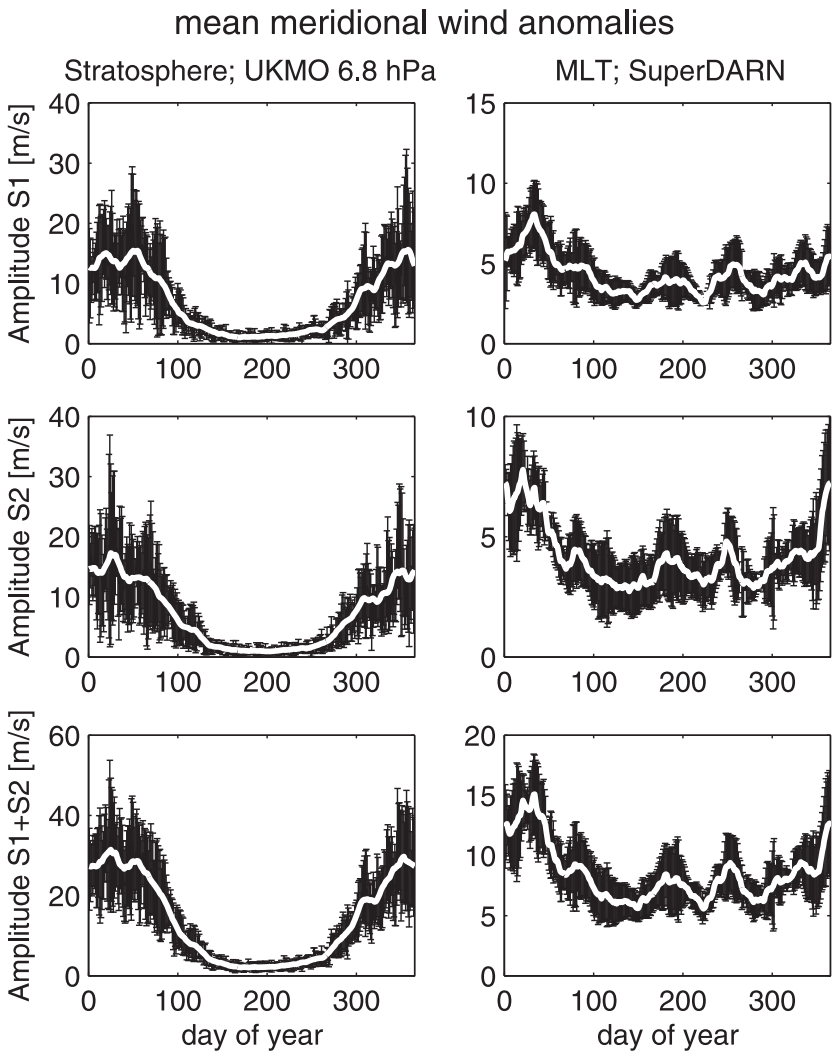

Figure 8. (left) Stratospheric planetary wave climatology from UKMO and (right) mesospheric planetary wave climatology from SuperDARN radar chain derived from the mean meridional wind anomalies. The white line shows the climatology of the 15 day smoothed (top) S_1, (middle) S_2 and (bottom) the sum of both. The black error bars depict the year-to-year variability of the zonal wave numbers.

during that winter [*Angell et al.*, 2006], as suggested by *Holton and Tan* [1980]. Furthermore, a persistent eastward traveling S_2 zonal wave packet in the mesosphere intensifies just before the start of the major stratospheric warming event that occurred in January/February 2006 (zonal wind reversal onset at 10hPa, 60°N on 21 January 2006). *Ushimaru and Tanaka* [1992] have shown that an eastward traveling S_2 planetary wave can interact with a strong stationary S_1 planetary wave in the stratosphere and create a major impact on the zonal mean flow there.

In contrast to the winter of 2005/2006, the mesospheric wave activity observed here during the winter of 2004/2005 is generally weaker, as can be seen in Figure 7 (right). Rather than a strong stationary S_1 component, this winter is characterized instead by a weaker westward traveling S_1 wave packet. Additionally, there is an absence of a strong eastward traveling S_2 component in January. This generally weak wave activity, as well as the absence of stationary S_1 and eastward traveling S_2 wave components in the mesosphere, is consistent with the anomalously strong polar vortex conditions observed during 2004/2005. This includes low stratospheric temperatures, ozone concentrations [*Angell et al.*, 2005], and the absence of a major stratospheric warming event [*Lima et al.*, 2012]. However, strong planetary wave activity in both wave numbers can be seen in mid-March during the final warming events. A more complete analysis of the MLT planetary wave evolution during major stratospheric warming events will be the subject of a future paper.

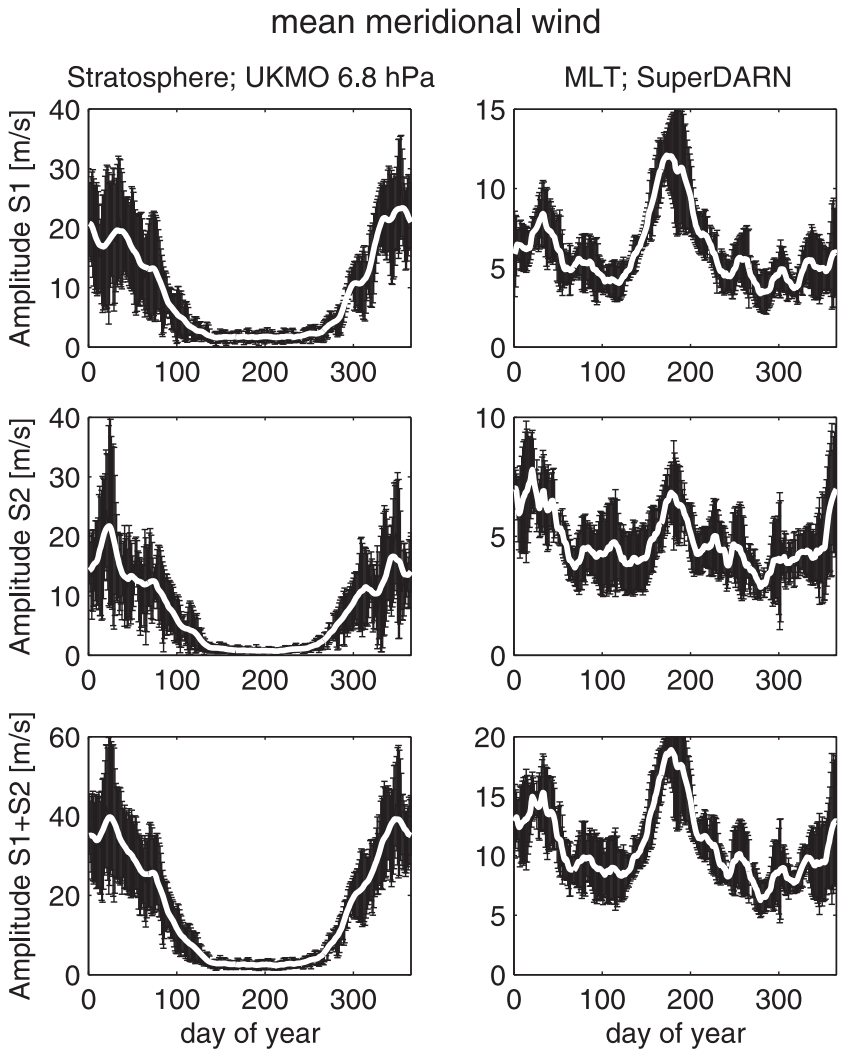

Figure 9. (left) Stratospheric planetary wave climatology from UKMO and (right) mesospheric planetary wave climatology from SuperDARN radar chain derived from the mean meridional wind. The white line shows the climatology of the 15 day smoothed (top) S_1, (middle) S_2, and (bottom) the sum of both. The black error bars depict the year-to-year variability of the zonal wave numbers.

5.2. Planetary Wave Climatologies

In order to examine the climatological seasonal behavior of the zonal wave numbers 1 and 2 components in both the stratosphere and the MLT, the daily average of the amplitudes retrieved in the fitting process were calculated. Climatologies (2000–2005) of planetary wave amplitudes fitted to the UKMO 6.8 hPa (~ 35 km) anomaly data at the radar stations are shown in Figure 8 (left) for the S_1, S_2 and the sum of S_1 and S_2. Similarly, climatologies (2000–2008) of wave amplitudes resulting form the fit to the SuperDARN radar anomaly winds are shown in the right-hand panels. The wave activity is smoothed with a 15 day running mean before averaging for better visibility of the general behavior.

In general the planetary wave activity of the zonal wave numbers 1 and 2 components has a similar magnitude and year-to-year variability. In the stratosphere (Figure 8 (left)) the planetary wave activity in both zonal wave numbers is low in summer and high in winter. This behavior reflects the filtering effect of the zonal background wind in the lower stratosphere. *Charney and Drazin* [1961] showed for a simplified, analytically solvable system that planetary waves can propagate only into regions where the zonal mean wind ($\bar{u}$) is both larger (more eastward) than the zonal velocity (c) of the wave and smaller (more westward) than the Rossby critical velocity (U_c), where U_c depends on the horizontal scale of the wave. The intrinsic wave velocity of Rossby waves is always westward and their propagation is therefore strongly prohibited by the stratospheric summertime westward jets. This explains the low values for both zonal wave numbers in the

summer stratosphere. The higher values in the winter stratosphere are related to general eastward zonal background winds and propagation of planetary waves from below. A strong year-to-year variability is visible during winter as has been observed in previous studies [e.g., *McDonald et al.*, 2011].

Large year-to-year variability can also be observed in the planetary wave activity of zonal wave numbers 1 and 2 in the MLT (Figure 8 (right)). The MLT magnitudes of both planetary wave zonal wave numbers are smaller than in the stratosphere. The seasonal variation of the MLT planetary wave activity is similar to that in the stratosphere but with smaller winter-summer ratios. In addition, the winter enhancement is more restricted in the MLT, generally occurring from late December until the beginning of March. This period represents times when stratospheric sudden warmings frequently occur in the Northern Hemisphere [e.g., *Manney et al.*, 2009a, 2009b; *Lima et al.*, 2012; *Matthias et al.*, 2012]. This supports the idea that sudden stratospheric warmings increase the vertical coupling. During sudden stratospheric warmings the stratospheric background wind is strongly reduced, or reversed during major events, and this favors the propagation of stratospheric planetary waves into the MLT.

In addition to the winter-time enhancement an increase in planetary wave activity can be seen during midsummer and around autumn equinox. Strong perturbations in the temperature near 87 km have been seen during the autumn equinox [*Taylor et al.*, 2001] and have been interpreted and modeled [*Liu et al.*, 2001] as an increase in planetary wave activity at these altitudes. The midsummer increase in planetary wave activity might be related to interhemispheric coupling above the strong summertime westward wind regime or to planetary wave generation in the upper atmosphere [e.g., *Williams and Avery*, 1992; *Forbes*, 1995; *Espy et al.*, 1997; *Mitchell et al.*, 1999; *Garcia et al.*, 2005; *Pancheva et al.*, 2008].

Figure 9 shows the climatologies of wave components for the mean meridional winds (station climatologies not removed). The seasonal behavior is similar to the climatology-removed case, with in general ∼15% higher amplitudes. The only exception is the MLT summer, where strong S_1 wave amplitudes appear. These high amplitudes are related to the stationary summertime wave feature seen in Figure 6 arising from the differences in the station climatologies seen in Figure 2. As mentioned before, this consistent wave feature can be interpreted as a result of longitudinal differences in gravity wave forcing [e.g., *Smith*, 2003].

6. Conclusion

Planetary wave activity in the MLT has been observed using meridional winds from the high northern latitude (51–66°N) SuperDARN network used as a "ground-based satellite." The zonal wave numbers 1 and 2 components have been extracted from daily mean meridional winds and wind anomalies from 25°E to 150°W for the years 2000–2008. The technique was validated over the entire data range by first using the wave components fitted over the entire longitude range to reconstruct the original observed wind at each individual station. The correlation between the reconstructions and the original data exceeded a correlation coefficient of 0.61, significant at >99% confidence level, for all stations. Further validation was done by applying the fit to meridional UKMO wind data at just the longitudes of the radar stations and comparing it to an ideal fit covering 360° (2.5° spacing) longitude. Finally, the planetary wave perturbation in the meridional wind at a single longitude derived from the SuperDARN chain was compared with an independent observation of OH-airglow temperatures over Stockholm. All three validation techniques indicate that the longitudinal fitting method applied to the SuperDARN meridional wind data is able to extract accurate planetary wave amplitudes that account for 40%–60% of the variation seen in the wind.

The climatology of planetary wave activity of zonal wave numbers 1 and 2 in the MLT (from SuperDARN) and stratosphere (from UKMO) indicates vertical coupling throughout the middle atmosphere around the autumn equinox and during winter when sudden stratospheric warming events occur frequently. The planetary wave amplitudes observed during winter are approximately halved between the stratosphere (∼ 35 km) and the MLT, indicating significant planetary wave energy dissipation in the middle atmosphere. Thus, the use of this method provides a way of monitoring the planetary wave activity in the MLT during stratospheric sudden warmings allowing a better understanding of stratospheric warming effects and mesospheric precursors [*Lee et al.*, 2009; *Manney et al.*, 2009b; *Kurihara et al.*, 2010; *Coy et al.*, 2011]. Finally, the difference between the mesospheric and stratospheric planetary wave activity during the summer indicates that any MLT wave activity due to transfer of planetary wave activity from the winter hemisphere [*Forbes*, 1995] occurs above the stratopause. However, it is also consistent with the regeneration of planetary waves in the

MLT due to the forcing by breaking gravity waves whose transmission through the stratosphere have been modulated by planetary waves in the lower stratosphere [*Holton*, 1984].

The SuperDARN chain is capable of providing a reliable measure of mesospheric planetary wave activity, allowing a quantitative assessment of wave strength, propagation direction, and evolution throughout the season. Furthermore, as the availability of SuperDARN and other wind measurements grows in both hemispheres, the method will be an important tool in assessing interhemispheric coupling.

Acknowledgments
The authors acknowledge the use of SuperDARN data. SuperDARN is a collection of radars funded by the national scientific funding agencies of Australia, Canada, China, France, Japan, South Africa, United Kingdom, and United States of America. The UK Meteorological Office assimilated data set was made available by the stratospheric British Atmospheric Data Centre. The authors are thankful for constructive comments provided during review.

References

Alexander, S. P., and M. G. Shepherd (2010), Planetary wave activity in the polar lower stratosphere, *Atmos. Chem. Phys.*, *10*(2), 707–718.

Angell, J. K., L. T. Flynn, M. E. Gelman, D. Hofmann, C. S. Long, A. J. Miller, and S. Zhou (2005), *Northern Hemisphere Winter Summary*, Oltmans, S. http://www.cpc.ncep.noaa.gov/products/stratosphere/winter_bulletins/nh_04-05/.

Angell, J. K., L. T. Flynn, M. E. Gelman, D. Hofmann, C. S. Long, A. J. Miller, S. Oltmans, and S. Zhou (2006), *Northern Hemisphere Winter Summary*. http://www.cpc.ncep.noaa.gov/products/stratosphere/winter_bulletins/nh_05-06/.

Arnold, N. F., P. A. Cook, T. R. Robinson, M. Lester, P. J. Chapman, and N. Mitchell (2003), Comparison of D-region Doppler drift winds measured by the SuperDARN Finland HF radar over an annual cycle using the Kiruna VHF meteor radar, *Ann. Geophys.*, *21*(10), 2073–2082.

Bancalá, S., K. Krüger, and M. Giorgette (2012), The preconditioning of major sudden stratospheric warmings, *J. Geophys. Res.*, *117*, D04101, doi:10.1029/2011JD016769.

Baumgaertner, A. J. G., A. J. McDonald, R. E. Hibbins, D. C. Fritts, D. J. Murphy, and R. A. Vincent (2008), Short-period planetary waves in the Antarctic middle atmosphere, *J. Atmos. Solar-Terr. Phys.*, *70*(10), 1336–1350, doi:10.1016/j.jastp.2008.04.007.

Belova, A. (2008), Studies of planetary waves in ozone and temperature fields as observed by the Odin satellite in 2002–2007, *IRF Scientific Report*, *298*, 35.

Belova, A., S. Kirkwood, D. Murtagh, N. Mitchell, W. Singer, and W. Hocking (2008), Five-day planetary waves in the middle atmosphere from Odin satellite data and ground-based instruments in Northern Hemisphere summer 2003, 2004, 2005 and 2007, *Ann. Geophys.*, *26*(11), 3557–3570.

Bristow, W. A., J. H. Yee, X. Zhu, and R. A. Greenwald (1999), Simultaneous observations of the July 1996 2-day wave event using the Super Dual Auroral Radar Network and the High Resolution Doppler Imager, *J. Geophys. Res.*, *104*(A6), 12,715–12,721, doi:10.1029/1999JA900030.

Charney, J. G., and P. G. Drazin (1961), Propagation of planetary-scale disturbance from lower into upper atmophere, *Geophys. Res. Lett.*, *66*(1), 83–109.

Chisham, G., and M. P. Freeman (2013), A reassessment of SuperDARN meteor echoes from the upper mesosphere and lower thermosphere, *J. Atmos. Solar-Terr. Phys.*, *102*, 207–221, doi:10.1016/j.jastp.2013.05.018.

Chshyolkova, T., A. H. Manson, and C. E. Meek (2005), Climatology of the quasi two-day wave over Saskatoon (52 degrees N, 107 degrees W): 14 Years of MF radar observations, in *Coupling Process in the MLT Region, Advances in Space Research*, vol. 35, edited by B. Clemesha and M. Taylor, pp. 2011–2016, 35th COSPAR Scientific Assembly, Paris, FRANCE, doi:10.1016/j.asr.2005.03.040.

Chshyolkova, T., A. H. Manson, C. E. Meek, S. K. Avery, D. Thorsen, J. W. MacDougall, W. Hocking, Y. Murayama, and K. Igarashi (2006), Planetary wave coupling processes in the middle atmosphere (30–90 km): A study involving MetO and MFR data, *J. Atmos. Solar-Terr. Phys.*, *68*(3–5), 353–368, doi:10.1016/j.jastp.2005.05.011.

Coy, L., S. D. Eckermann, K. W. Hoppel, and F. Sassi (2011), Mesospheric precursors to the major stratospheric sudden warming of 2009: Validation and dynamical attribution using a ground-to-edge-of-space data assimilation system, *J. Adv. Model. Earth Syst.*, *3*(4), M10002, doi:10.1029/2011MS000067.

Demissie, T. D., N. H. Kleinknecht, R. E. Hibbins, P. J. Espy, and C. Straub (2013), Quasi-16 day planetary-wave oscillations observed in ozone and temperature data from Antarctica, *Ann. Geophys.*, *31*, 1–6, doi:10.5194/angeo-31-1-2013.

Dowdy, A. J., R. A. Vincent, M. Tsutsumi, K. Igarashi, Y. Murayama, W. Singer, and D. J. Murphy (2007), Polar mesosphere and lower thermosphere dynamics: Mean wind and gravity wave climatologies, *J. Geophys. Res.*, *112*, D17104, doi:10.1029/2006JD008126.

Dowdy, A. J., R. A. Vincent, D. J. Murphy, M. Tsutsumi, D. M. Riggin, and M. J. Jarvis (2004), The large-scale dynamics of the mesosphere-lower thermosphere during the Southern Hemisphere stratospheric warming of 2002, *Geophys. Res. Lett.*, *31*, L14102, doi:10.1029/2004GL020282.

Espy, P. J., J. Stegman, and G. Witt (1997), Interannual variations of the quasi-16-day oscillation in the polar summer mesospheric temperature, *J. Geophys. Res.*, *102*(D2), 1983–1990, doi:10.1029/96JD02717.

Espy, P. J., R. E. Hibbins, D. M. Riggin, and D. C. Fritts (2005), Mesospheric planetary waves over Antarctica during 2002, *Geophys. Res. Lett.*, *32*, L21804, doi:10.1029/2005GL023886.

Forbes, J. M. (1995), Tidal and planetary waves, in *The Upper Mesosphere and Lower Thermosphere: A Review of Experiment and Theory, Geophys. Monogr. Ser.*, vol. 87, pp. 67–87, AGU, Washington, D. C.

Garcia, R. R., R. Lieberman, J. M. Russell, and M. G. Mlynczak (2005), Large-scale waves in the mesosphere and lower thermosphere observed by SABER, *J. Atmos. Sci.*, *62*(12), 4384–4399, doi:10.1175/JAS3612.1.

Greenwald, R. A., K. B. Baker, R. A. Hutchins, and C. Hanuise (1985), An HF phase-array radar for studying small-scale structure in the high-latitude ionosphere, *Radio Sci.*, *20*(1), 63–79, doi:10.1029/RS020i001p00063.

Greenwald, R. A., et al. (1995), DARN/SUPERDARN—A global view of the dynamics of high-latitude convection, *Space Sci. Rev.*, *71*(1–4), 761–796, doi:10.1007/BF00751350.

Grytsai, A., Z. Grytsai, A. Evtushevsky, G. Milinevsky, and N. Leonov (2005), Zonal wave numbers 1–5 in planetary waves from the TOMS total ozone at 65 degrees S, *Ann. Geophys.*, *23*(5), 1565–1573.

Hall, G. E., J. W. MacDougall, D. R. Moorcroft, J. P. St.-Maurice, A. H. Manson, and C. E. Meek (1997), Super Dual Auroral Radar Network observations of meteor echoes, *J. Geophys. Res.*, *102*(A7), 14,603–14,614, doi:10.1029/97JA00517.

Hibbins, R. E., and M. J. Jarvis (2008), A long-term comparison of wind and tide measurements in the upper mesosphere recorded with an imaging Doppler interferometer and SuperDARN radar at Halley, Antarctica, *Atmos. Chem. Phys.*, *8*(5), 1367–1376, doi:10.5194/acp-8-1367-2008.

Hibbins, R. E., P. J. Espy, and M. J. Jarvis (2006), Mean winds and tides in the mesosphere and lower thermosphere above Halley, Antarctica, *J. Atmos. Solar-Terr. Phys.*, *68*(3–5), 436–444, doi:10.1016/j.jastp.2005.02.030.

Hibbins, R. E., M. P. Freeman, S. E. Milan, and J. M. Ruohoniemi (2011), Winds and tides in the mid-latitude Southern Hemisphere upper mesosphere recorded with the Falkland Islands SuperDARN radar, *Ann. Geophys.*, *29*(11), 1985–1996, doi:10.5194/angeo-29-1985-2011.

Hocking, W. K., B. Fuller, and B. Vandepeer (2001), Real-time determination of meteor-related parameters utilizing modem digital technology, *J. Atmos. Solar-Terr. Phys.*, *63*(2–3), 155–169, doi:10.1016/S1364-6826(00)00138-3.

Holton, J. R. (1984), The generation of mesospheric planetary-waves by zonally asymmetric greavity-wave breaking, *J. Atmos. Sci.*, *41*(23), 3427–3430, doi:10.1175/1520-0469(1984)041<3427:TGOMPW>2.0.CO;2.

Holton, J. R., and H. C. Tan (1980), The influenced of the equatorial quasi-biennial oscillation on the global circulation at 50 mb, *J. Atmos. Sci.*, *37*(10), 2200–2208, doi:10.1175/1520-0469(1980)037<2200:TIOTEQ>2.0.CO;2.

Hussey, G. C., C. E. Meek, D. Andre, A. H. Manson, G. J. Sofko, and C. M. Hall (2000), A comparison of Northern Hemisphere winds using SuperDARN meteor trail and MF radar wind measurements, *J. Geophys. Res.*, *105*(D14), 18,053–18,066, doi:10.1029/2000JD900272.

Jarvis, M. J., G. O. L. Jones, and B. Jenkins (1999), New initiatives in observing the Antarctic mesosphere, *Adv. Space Res.*, *24*(5), 611–619, doi:10.1016/S0273-1177(99)00479-2.

Jenkins, B., and M. J. Jarvis (1999), Mesospheric winds derived from SuperDARN HF radar meteor echoes at Halley, Antarctica, *Earth Planets Space*, *51*(7–8), 685–689.

Jenkins, B., M. J. Jarvis, and D. M. Forbes (1998), Mesospheric wind observations derived from Super Dual Auroral Radar Network (SuperDARN) HF radar meteor echoes at Halley, Antarctica: Preliminary results, *Radio Sci.*, *33*(4), 957–965, doi:10.1029/98RS01113.

Kurihara, J., Y. Ogawa, S. Oyama, S. Nozawa, M. Tsutsumi, C. M. Hall, Y. Tomikawa, and R. Fujii (2010), Links between a stratospheric sudden warming and thermal structures and dynamics in the high-latitude mesosphere, lower thermosphere, and ionosphere, *Geophys. Res. Lett.*, *37*, L13806, doi:10.1029/2010GL043643.

Labitzke, K. (1977), Innerannual variability of the winter stratosphere in the northern hemisphere, *Mon. Weather Rev.*, *105*, 762–770.

Labitzke, K. (1981), The amplification of height wave 1 in January 1979: A characteristic precondition for major warming in February, *Mon. Weather Rev.*, *109*, 983–989.

Lee, J. N., D. L. Wu, G. L. Manney, and M. J. Schwartz (2009), Aura microwave limb sounder observations of the northern annular mode: From the mesosphere to the upper troposphere, *Geophys. Res. Lett.*, *36*, L20807, doi:10.1029/2009GL040678.

Lima, L. M., E. O. Alves, P. P. Batista, B. R. Clemesha, A. F. Medeiros, and R. A. Buriti (2012), Sudden stratospheric warming effects on the mesospheric tides and 2-day wave dynamics at 7 degrees S, *J. Atmos. Solar-Terr. Phys.*, *78–79*(SI), 99–107, doi:10.1016/j.jastp.2011.02.013.

Lindzen, R. S. (1981), Turbulence and stress owing to gravity wave and tidal breakdown, *J. Geophys. Res.*, *86*, 9707–9714.

Liu, H. L., R. G. Roble, M. J. Taylor, and W. R. Pendleton Jr. (2001), Mesospheric planetary waves at northern hemisphere fall equinox, *Geophys. Res. Lett.*, *28*, 1903–1906.

Manney, G. L., et al. (2009a), Satellite observations and modeling of transport in the upper troposphere through the lower mesosphere during the 2006 major stratospheric sudden warming, *Atmos. Chem. Phys.*, *9*(14), 4775–4795, doi:10.5194/acp-9-4775-2009.

Manney, G. L., M. J. Schwartz, K. Krüger, M. L. Santee, S. Pawson, J. N. Lee, W. Daffer, R. A. Fuller, and N. J. Livesey (2009b), Aura microwave limb sounder observations of dynamics and transport during the record-breaking 2009 arctic stratospheric major warming, *Geophys. Res. Lett.*, *36*, L12815, doi:10.1029/2009GL038586.

Manson, A. H., C. E. Meek, M. J. Smith, and G. J. Fraser (1985), Direct comparisons of prevailing winds and tital wind fiels (24-h, 12-h) in the upper middle armosphere(60–105 km) during 1978–1980 Saskatoon (52-degrees-n, 107-degrees-w) and Christchurch (44-degrees-s, 173-degree-e), *J. Atmos. Terr. Phys.*, *47*(5), 463–476, doi:10.1016/0021-9169(85)90112-6.

Matthias, V., P. Hoffmann, M. Rapp, and G. Baumgarten (2012), Composite analysis of the temporal development of waves in the polar MLT region during stratospheric warmings, *J. Atmos. Solar-Terr. Phys.*, *90–91*(SI), 86–96, doi:10.1016/j.jastp.2012.04.004.

McDonald, A. J., R. E. Hibbins, and M. J. Jarvis (2011), Properties of the quasi 16 day wave derived from EOS MLS observations, *J. Geophys. Res.*, *116*, D06112, doi:10.1029/2010JD014719.

Met Office et al. (2013), Stratospheric assimilated data, [internet], NCAS British Atmospheric Data Centre, 2006, Available from http://badc.nerc.ac.uk/view/badc.nerc.ac.uk__ATOM__dataent_ASSIM.

Milan, S. E., T. B. Jones, T. R. Robinson, E. C. Thomas, and T. K. Yeoman (1997), Interferometric evidence for the observation of ground backscatter originating behind the cutlass coherent hf radars, *Ann. Geophys.*, *15*, 29–39, doi:10.1007/s00585-997-0029-y.

Mitchell, N. J., H. R. Middleton, A. G. Beard, P. J. S. Williams, and H. G. Muller (1999), The 16-day planetary wave in the mesosphere and lower thermosphere, *Ann. Geophys.*, *17*, 1447–1456, doi:10.1007/s00585-999-1447-9.

Mitchell, N. J., D. Pancheva, H. R. Middleton, and M. E. Hagan (2002), Mean winds and tides in the Arctic mesosphere and lower thermosphere, *J. Geophys. Res.*, *107*(A1), 1004, doi:10.1029/2001JA900127.

Pancheva, D., et al. (2008), Planetary waves in coupling the stratosphere and mesosphere during the major stratospheric warming in 2003/2004, *J. Geophys. Res.*, *113*, D12105, doi:10.1029/2007JD009011.

Portnyagin, Y. I., et al. (2004), Monthly mean climatology of the prevailing winds and tides in the Arctic mesosphere/lower thermosphere, *Ann. Geophys.*, *22*(10), 3395–3410.

Salby, M. L. (1981), The 2-day wave in the middle atmophere: Observations and theory, *J. Geophys. Res.*, *86*(C10), 9654–9660, doi:10.1029/JC086iC10p09654.

Smith, A. K. (2003), The origion of stationary planetary waves in the upper mesosphere, *J. Atmos. Sci.*, *60*, 3033–3041.

Stearns, S. D. (1975), *Digital signal analysis*, Hayden book, Rochelle Park, New Jersey.

Swinbank, R., and A. A. O'Neill (1994), A stratosphere-troposphere data assimilation system, *Mon. Weather Rev.*, *122*, 686–702.

Taylor, M. J., W. R. Pendleton Jr., H. L. Liu, C. Y. She, L. C. Garnet, R. G. Roble, and V. Vasoli (2001), Large amplitude pertubationa in the mesospheric OH meinel and 87-km Na lidar temperatures around the autumnal equinox, *Geophys. Res. Lett.*, *28*, 1899–1902.

Thayaparan, T., and W. K. Hocking (2002), A long-term comparison of winds and tides measured at London, Canada (43N, 81W) by co-located MF and meteor radars, *J. Atmos. Solar-Terr. Phys.*, *64*(8–11), 931–946, doi:10.1016/S1364-6826(02)00048-2.

Tsutsumi, M., A. S. Yukimatu, D. A. Holdsworth, and M. Lester (2009), Advanced SuperDARN meteor wind observations based on raw time series analysis technique, *Radio Sci.*, *44*, RS2006, doi:10.1029/2008RS003994.

Ushimaru, S., and H. Tanaka (1992), A numerical study of the interaction between stationary rossby waves and eastward-traveling waves in the southern hemisphere stratosphere, *J. Atmos. Sci.*, *49*(15), 1354–1373, doi:10.1175/1520-0469(1992)049<1354:ANSOTI>2.0.CO;2.

Williams, C. R., and S. K. Avery (1992), Analysis of long-period waves using the mesosphere-stratosphere-troposphere radar at Poker Flat, Alaska, *J. Geophys. Res.*, *97*(D18), 20,855–20,861.

Wu, D. L., P. B. Hays, and Wilbert R. S. (1995), A least-squares method for spectral-analysis of space-time series, *J. Atmos. Sci.*, *52*(20), 3501–3511, doi:10.1175/1520-0469(1995)052<3501:ALSMFS>2.0.CO;2.

Yukimatu, A. S., and M. Tsutsumi (2002), A new SuperDARN meteor wind measurement: Raw time series analysis method and its application to mesopause region dynamics, *Geophys. Res. Lett.*, *29*(20), 1981, doi:10.1029/2002GL015210.